Heat Balance in the Pacific Warm Pool Atmosphere during TOGA COARE and CEPEX

BAIJUN TIAN, GUANG JUN ZHANG, AND V. RAMANATHAN

Center for Atmospheric Sciences, Center for Clouds, Chemistry and Climate, Scripps Institution of Oceanography, University of California, San Diego, La Jolla, California

(Manuscript received 30 September 1999, in final form 25 April 2000)

ABSTRACT

The atmosphere above the western equatorial Pacific warm pool (WP) is an important source for the dynamic and thermodynamic forcing of the atmospheric general circulation. This study uses a high-resolution reanalysis and several observational datasets including Global Precipitation Climatology Project precipitation, Tropical Ocean Global Atmosphere (TOGA) Tropical Atmosphere Ocean moored buoys, and Earth Radiation Budget Experiment, TOGA Coupled Ocean–Atmosphere Response Experiment (COARE), and Central Equatorial Pacific Experiment (CEPEX) radiation data to examine the details of the dynamical processes that lead to this net positive forcing. The period chosen is the period of two field experiments: TOGA COARE and CEPEX during December 1992–March 1993.

The four months used in the study were sufficient to establish that the warm pool atmosphere (WPA) was close to a state of radiative–convective–dynamic equilibrium. The analysis suggests that the large-scale circulation imports about 200 W m^{-2} of sensible heat and about 140 W m^{-2} of latent energy into the WPA mainly through the low-level mass convergence and exports about 420 W m^{-2} potential energy mainly through the upper-level mass divergence. Thus the net effect of the large-scale dynamics is to export about 80 W m^{-2} energy out of the WPA and cool the WPA by about 0.8 K day^{-1}. The dynamic cooling in addition to the radiative cooling of about 0.4 K day^{-1} or 40 W m^{-2} leads to a net radiative–dynamic cooling of about 1.2 K day^{-1} or 120 W m^{-2}, which should be balanced by convective heating of the same magnitude.

The WPA radiative cooling is only about 0.4 K day^{-1}, which is considerably smaller than previously cited values in the Tropics. This difference is largely due to the cloud radiative forcing (CRF), about 70 W m^{-2}, associated with the deep convective cirrus clouds in the WPA, which compensates the larger clear sky radiative cooling. Thus moist convection heats the WPA, not only through the direct convective heating, that is, the vertical eddy sensible heat and latent energy transport, but also through the indirect convective heating, that is, the CRF of deep convective clouds. The CRF of the deep convective clouds has a dipole structure, in other words, strong heating of the atmosphere through convergence of longwave radiation and a comparable cooling of the surface through the reduction of shortwave radiation at the surface. As a result, the deep convective clouds enhance the required atmospheric heat transport and reduce the required oceanic heat transport significantly in the WP. A more detailed understanding of these convective processes is required to improve our understanding of the heat transport by the large-scale circulation in the Tropics.

1. Introduction

The western equatorial Pacific warm pool (WP) contains the largest body of warm water found in the planet with annual mean sea surface temperature (SST) exceeding 302 K. The WP atmosphere (WPA) is an important source for the dynamic and thermodynamic forcing of the atmospheric general circulation and it plays a central role in the El Niño–Southern Oscillation phenomena (Webster and Lukas 1992). A primary objective of the Tropical Ocean Global Atmosphere Coupled Ocean–Atmosphere Response Experiment (TOGA COARE; Webster and Lukas 1992; Godfrey et al. 1998) and the Central Equatorial Pacific Experiment (CEPEX; Ramanathan et al. 1993) was to carefully observe and better understand ocean–atmosphere coupling in the WP. In spite of its importance, we have not yet developed a sound understanding of the physical processes that govern the extent, the depth, and the SST of the WP. And the successful simulation of the WP still remains an elusive goal. Most of the studies concerning the regulation of SST in the WP assume that the large-scale atmospheric circulation is very efficient in exporting heat out of the WPA (e.g., Ramanathan and Collins 1991; Fu et al. 1992; Wallace 1992; Hartmann and Michelsen 1993; Lau et al. 1994; Pierrehumbert 1995). Yet none of these studies have addressed how the large-

Corresponding author address: V. Ramanathan, Center for Clouds, Chemistry and Climate, Scripps Institution of Oceanography, University of California, San Diego, 9500 Gilman Dr., La Jolla, CA 92093-0239.
E-mail: ram@fiji.ucsd.edu

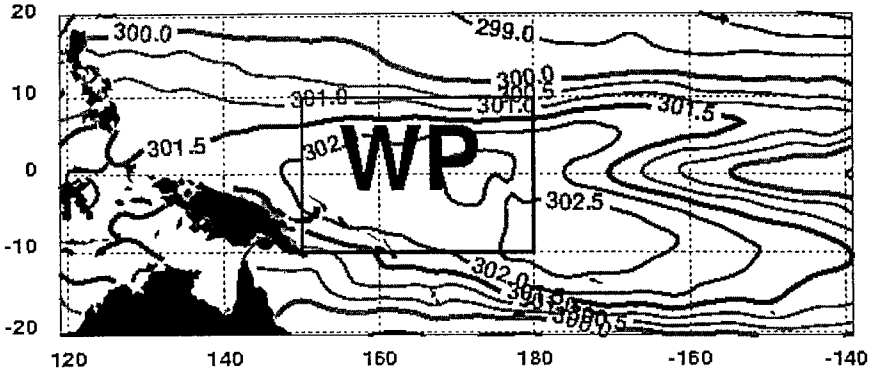

FIG. 1. The 4-month average (from Dec 1992 to Mar 1993, the same latter) SST from the FSU reanalysis. This unit is K. The Pacific warm pool (WP) used for this study extends from 150°E to 180° and from 10°S to 10°N, which crudely corresponds to the TOGA COARE large-scale array (LSA).

scale circulation exports heat. The purpose of this study is to understand the role of the large-scale dynamics in the WP atmospheric heat balance and the overall heat balance picture in the WPA.

Several previous studies on the tropical heat balance are relevant to our work. Riehl and Malkus (1958, 1979) studied the heat balance in the equatorial trough zone. They found that the equatorial trough zone receives the latent heat accumulated by the lower trades. As the air is lifted in the trough zone, latent energy is converted to sensible heat and potential energy to balance the radiation losses. The residue is exported poleward aloft in the form of sensible heat and potential energy. Riehl and Malkus (1958, 1979) also found that in the equatorial trough zone, due to the radiative cooling and the heat transport by the gradual mass circulation, the upper troposphere cools at a rate of about 2 K day^{-1}. To compensate for this cooling, they proposed a mechanism in which buoyant parcels rise in undiluted hot towers, compensated mass-wise by the downdrafts. It is shown that a total of 1500–5000 active undiluted hot towers around the globe in the equatorial trough zone are required to balance that heat loss. Oort (1971) and Oort and Peixoto (1983) studied the atmospheric heat transport using the global rawinsonde network data and the daily ship reports. In the Tropics, they found that both the latent energy and the sensible heat transport are equatorward, while the potential energy flux is poleward. The energy flux due to both transient and standing eddies is practically negligible equatorward of 10° and 15° lat. Trenberth and Solomon (1994) computed the heat budget locally over the entire globe for 1988 using the Earth Radiation Budget Experiment (ERBE; Barkstrom 1984) data and the European Centre for Medium-Range Weather Forecasts (ECMWF) atmospheric data. They found that the atmospheric heat transport in the western tropical Pacific is about 80 W m^{-2} for January 1988. The large-scale atmospheric circulation imports the latent energy and exports the dry static energy out of the tropical Pacific mainly through the stationary divergent component. To what extent are these results applicable to the western equatorial Pacific WP? Specifically, what is the role of the large-scale atmospheric circulation in the WP atmospheric heat budget? How is the energy exported out of the WPA? What is the overall heat balance picture in the WPA? We will address these questions with the new datasets available for the TOGA COARE and CEPEX period, that is, from December 1992 to March 1993. The western equatorial Pacific WP domain in this study extends from 150°E to 180° and from 10°S to 10°N (Fig. 1). This approximately coincides with the TOGA COARE large-scale array (LSA; Webster and Lukas 1992), where tremendous observational datasets are available from TOGA COARE and CEPEX.

The basic organization of this paper is as follows. The data used in this study are described in section 2. Section 3 presents the heat budget equations and the analysis methods. The results about the WP large-scale atmospheric heat transport mechanism are shown in section 4. In section 5, we analyze the WPA heat source and synthesize the energy cycle. The uncertainties in the data and analyses are discussed in section 6. The main conclusions and the overall heat balance picture in the WPA are summarized in the last section.

2. Data

To evaluate the large-scale atmospheric heat transport in the WPA, high-spatial and temporal resolution dynamic and thermodynamic data are required. The radiosonde network observations during TOGA COARE and CEPEX are not enough for this purpose. Fortunately, a very high-resolution reanalysis covering the period of TOGA COARE, CEPEX from December 1992 to March 1993 was done by Florida State University (FSU) using a high-resolution global spectral model (Krishnamurti et al. 1997). The reanalysis is based on physical analysis procedures developed at FSU (Krishnamurti et al. 1991). The observed rainfall used during

the physical initialization was based on surface and satellite rainfall as described in Gairola and Krishnamurti (1992). The physical initialization involves rainfall and outgoing longwave radiation (OLR) assimilation using several reverse algorithms: a reverse cumulus parameterization, a reverse surface similarity, and a matching of the OLR where the model-based values are relaxed toward satellite based values. The entire process restructures the humidity profiles along the vertical and spins up the convective heating, divergence, and the related fields consistent with the observed rain rates. The unique aspects of this reanalysis are the following: (i) It incorporates the physical initialization. (ii) It has a very high-spatial resolution, that is, the horizontal resolution is triangular 170 waves (roughly 70 km at the equator) and the vertical resolution is 15 layers between roughly 10 and 1000 mb. (iii) The ECMWF reanalysis was used as a first guess field. (iv) This is a four times daily dataset, which can capture the diurnal cycle and has a high-temporal resolution. This global dataset consists of all the basic and derived meteorological variables and is the major dataset for this study.

Several other observational datasets are also used in this study in order to close the heat budget and check the reliability of the heat budget calculation based on the FSU reanalysis. The Global Precipitation Climatology Project (GPCP; Arking and Xie 1994) version 1a combined precipitation dataset (Huffman et al. 1997; ftp://ftp.ncdc.noaa.gov/pub/data/gpcp/version1/) is used to provide independent estimates of precipitation. It is a 2.5° × 2.5° gridded, monthly mean precipitation dataset covering the period from July 1987 to June 1997. It employs four methods to estimate the global rainfall: Special Sensor and Microwave/Image, OLR, rain gauge, and numerical model. The moored buoy data from the TOGA Tropical Atmosphere Ocean (TAO; Hayes et al. 1991; http://www.pmel.noaa.gov/tao) are used to estimate the surface turbulent fluxes (e.g., Zhang and McPhaden 1995). The ERBE data from the wide field of view (WFOV) instrument (http://eosweb.larc.nasa.gov/HPBIN/grow.pl?+ERBE#ERBE) during COARE and CEPEX period is used to estimate the radiative flux at the top of the atmosphere (TOA). The surface radiation budget is from TOGA COARE and CEPEX observations (e.g., Collins et al. 1996; Chou et al. 1998).

3. Methodology

a. Heat budget equations

The energy or heat in the atmosphere is usually considered in the form of sensible heat c_pT, potential energy $\Phi = gz$, latent energy Lq, and kinetic energy $k = \frac{1}{2}(u^2 + v^2)$. Because of its small value, the kinetic energy can be neglected in the total heat budget (e.g., Riehl and Malkus 1958, 1979; Oort 1971; Oort and Peixoto 1983; Peixoto and Oort 1992). Using the equation of state, the continuity equation, and the hydrostatic equation, the large-scale atmospheric sensible heat, potential energy, and latent energy equations can be written as

$$\frac{\partial}{\partial t}(c_pT) + \nabla\cdot(c_pT\mathbf{v}) + \frac{\partial}{\partial p}(c_pT\omega) - \omega\alpha = Q_1 = Q_R + L(c - e) - \frac{\partial}{\partial p}\overline{(c_pT'\omega')}, \quad (1)$$

$$\frac{\partial\Phi}{\partial t} + \nabla\cdot(\Phi\mathbf{v}) + \frac{\partial}{\partial p}(\Phi\omega) + \omega\alpha = 0, \quad (2)$$

$$\frac{\partial}{\partial t}(\mathrm{Lq}) + \nabla\cdot(\mathrm{Lq}\mathbf{v}) + \frac{\partial}{\partial p}(\mathrm{Lq}\omega) = -Q_2 = -\left[L(c - e) + \frac{\partial}{\partial p}\overline{(\mathrm{Lq}'\omega')}\right], \quad (3)$$

where $c - e$ is the net condensation of water vapor per unit mass, L is the latent heat of vaporization, and Q_1 and Q_2 are referred to as the apparent heat source and the apparent moisture sink in the atmosphere by Yanai et al. (1973). For simplicity, the role of liquid water in the atmosphere is ignored in this paper.

Combining Eqs. (1)–(3) gives the large-scale atmospheric moist static energy equation,

$$\frac{\partial h}{\partial t} + \nabla\cdot(h\mathbf{v}) + \frac{\partial}{\partial p}(h\omega) = Q = Q_R + Q_C, \quad (4)$$

where $h = s + \mathrm{Lq} = c_pT + \Phi + \mathrm{Lq}$ is moist static energy and it is also called ''total heat'' or ''total energy'' in this paper. Here $s = c_pT + \Phi$ is dry static energy. The term $\nabla\cdot(h\mathbf{v}) + (\partial/\partial p)(h\omega)$ represents the heat transport by the large-scale atmospheric circulation, and $Q = Q_1 - Q_2 = Q_R + Q_C$ is the apparent total heat source in the atmosphere, which includes radiative heating Q_R and convective heating $Q_C = -(\partial/\partial p)\overline{(h'\omega')}$. Following Yanai et al. (1973), it will be assumed that the small-scale eddies in the horizontal components of wind have no significant correlations with c_pT', Φ', and Lq'. But because of the presence of cumulus convection and turbulence, the vertical eddy transport of sensible heat and latent energy can be significant. We refer to this vertical eddy transport of sensible heat and latent energy by the cumulus convection and turbulence as the convective heating or the direct convective heating as opposed to the indirect convective heating, that is, the cloud radiative forcing (CRF) of deep convective clouds. Overbar represents grid mean or large-scale variable, and prime represents the deviation from the mean. For clarity, overbars have been omitted in Eqs. (1)–(4) except for the convective terms. Equations (1)–(4) form the basic set of equations to be used in this study.

On the seasonal timescale, the heat storage term is close to zero and the WPA is in equilibrium, so the large-scale atmospheric total heat budget Eq. (4) can be rewritten as

$$Q_R + Q_C + Q_D = 0, \quad (5)$$

where $Q_D = -[\nabla \cdot (h\mathbf{v}) + (\partial/\partial p)(h\omega)]$ denotes the dynamic heating due to the heat transport by the large-scale atmospheric circulation. Equation (5) shows that the WPA is in a state of radiative-convective-dynamic equilibrium. The roles of the large-scale dynamics, radiation, and convection in the WP atmospheric heat budget are discussed separately in the next two sections. The role of the large-scale dynamics is our focus.

b. Analysis methods

To compute the large-scale dynamic heat transport in the WPA, we integrate Eqs. (1)–(4) over the atmospheric column from the surface to the TOA:

$$\frac{\partial}{\partial t}\overline{\overline{(c_pT)}} + \nabla \cdot \overline{\overline{(c_pT\mathbf{v})}} - \overline{\overline{(\omega\alpha)}} = \overline{\overline{Q}}_1 = R_T - R_S + \text{LP} + \text{SH}, \quad (6)$$

$$\frac{\partial}{\partial t}\overline{\overline{(\Phi)}} + \nabla \cdot \overline{\overline{(\Phi\mathbf{v})}} + \overline{\overline{(\omega\alpha)}} = 0, \quad (7)$$

$$\frac{\partial}{\partial t}\overline{\overline{(\text{Lq})}} + \nabla \cdot \overline{\overline{(\text{Lq}\mathbf{v})}} = -\overline{\overline{Q}}_2 = \text{LE} - \text{LP}, \quad (8)$$

$$\frac{\partial}{\partial t}\overline{\overline{(h)}} + \nabla \cdot \overline{\overline{(h\mathbf{v})}} = \overline{\overline{Q}} = R_T - R_S + \text{LE} + \text{SH}, \quad (9)$$

where $\overline{\overline{(\ )}} = (1/g)\int_0^{p_s}(\ )\,dp$ represents the mass-weighted vertical integral over the atmospheric column from the surface to the TOA. Here R_T, R_S is the net downward radiation flux at the TOA and at the surface, respectively, and $\text{LP} = \overline{\overline{[L(c-e)]}}$ is the latent heat release from precipitation. Also $\text{SH} = -(1/g)\overline{(c_pT'\omega')}|_{p_s}$ and $\text{LE} = -(1/g)\overline{(L\omega'q')}|_{p_s}$ are the surface sensible and latent heat flux, respectively.

The lhs of Eqs. (6)–(9) can be computed using the FSU fields. To check the accuracy of the budget calculation independently, we will use the observed radiative fluxes and precipitation from the satellite data and the surface sensible and latent heat fluxes from the TOGA TAO buoys to estimate the rhs of Eqs. (6)–(9).

The fields that characterize the state of the atmosphere are highly variable in time. However, climate is defined, to a large extent, by the average conditions, which suggests the use of averages over certain time intervals, such as monthly, seasonal, and yearly averages (e.g., Peixoto and Oort 1992). For a large-scale variable A, the time mean is defined as $\langle A\rangle = \int_{T1}^{T2} A\,dt/\int_{T1}^{T2} dt$ and the transient part is $A^* = A - \langle A\rangle$. In this study, the time mean corresponds to the monthly mean and the transients correspond to departures from it. So the large-scale dynamic fields can be divided into the monthly mean circulation (MMC) and the transient eddies (TEs), that is, $\mathbf{v} = \langle\mathbf{v}\rangle + \mathbf{v}^*$, where $\langle\mathbf{v}\rangle = (\langle u\rangle, \langle v\rangle)$ is the MMC, and $\langle v\rangle$ and $\langle u\rangle$ are the monthly mean meridional (Hadley) and zonal (Walker) circulation, respectively. Accordingly the monthly mean flux of A can be partitioned into MMC and TEs component:

$$\langle A\mathbf{v}\rangle = \langle A\rangle\langle\mathbf{v}\rangle + \langle A^*\mathbf{v}^*\rangle. \quad (10)$$

The first term is the monthly mean flux due to the MMC and the second term is the monthly mean flux contributed from the TEs.

The calculation of the large-scale atmospheric heat transport is very sensitive to the vertical p velocity especially in the upper troposphere because of the high static stability. Following Yanai and Tomita (1998), the vertical p velocity ω is calculated from the horizontal divergence and the mass continuity equation with the surface boundary condition

$$\omega_S = -\rho_S\,\mathbf{v}_S \cdot \nabla\Phi_S, \quad (11)$$

where ω_S, $\mathbf{v}_S$, and Φ_S are the surface vertical velocity, horizontal velocity, and geopotential, respectively, and ρ_S is the air density at the surface calculated using the equation of state: $\rho_s = p_s/R_dT_{vs}$. The TOA boundary condition is $\omega_T = 0$ at $p_T = 100$ mb. Considering that errors in the divergence field calculation are inevitable using the analysis data, the adjustment method introduced by Yanai and Tomita (1998) is used to correct the divergence field. The first guess of the divergence field at the layer midpoints, $D_0 = [1/(a\cos\varphi)][\partial u/\partial\lambda + (\partial/\partial\varphi)(v\cos\varphi)]$, is adjusted by adding

$$D' = \left(\omega_T - \omega_S - \int_{p_T}^{p_S} D_0\,dp\right)\Big/(p_s - p_T). \quad (12)$$

The corrected divergence field $D = D_0 + D'$ is used to obtain the adjusted values of the vertical p velocity and the energy transport at all levels.

The procedure for making the set of budget calculations in this study has been established rigorously in Trenberth (1997). That paper discussed several pitfalls one must avoid in handling analyzed fields. For example, Trenberth (1997) pointed out the difficulties in dealing with the lower boundary in the p-coordinate system because of complex orography. However, in this paper, we are primarily dealing with the WPA with virtually no orography. In addition, Trenberth (1997) noted that a balanced mass budget is essential for the energy budget calculation. In this paper, we follow the procedure suggested by Trenberth (1997).

4. Large-scale dynamic heat transport

a. Total heat transport

Using the FSU reanalysis over the 4-month period, we computed the total heat transport term $\langle\nabla \cdot \overline{\overline{(h\mathbf{v})}}\rangle$ and its contribution from sensible heat, potential energy, and latent energy. The results are summarized in Table 1. Averaged over the four months, the large-scale circulation exports about 60 W m^{-2} moist static energy out of the WPA, of which 160 W m^{-2} is in the form of

TABLE 1. The 4-month average (from Dec 1992 to Mar 1993, the same latter) monthly mean divergence of mass-weighted vertical integral of the large-scale dynamic moist static energy (h) flux in the WPA and its contributions from latent energy (Lq), sensible heat (c_pT), potential energy (ϕ), and dry static energy (s). The unit is W m^{-2}.

h	Lq	c_pT	ϕ	s
60	−100	−260	420	160

dry static energy export and −100 W m^{-2} is from latent energy flux convergence. These numbers are comparable to those of Trenberth and Solomon (1994), who deduced the atmospheric moist static, dry static, and latent energy transport in the WP to be about 80, 160, and −80 W m^{-2}, respectively for January 1988. Further partitioning revealed that the 160 W m^{-2} dry static energy export represents the sum of 420 W m^{-2} export of potential energy and −260 W m^{-2} import of sensible heat. Thus the large-scale circulation imports both latent energy and sensible heat into the WPA, and exports potential energy out of the WPA. The individual energy transport is large, however the strong compensation between potential energy transport and sensible heat plus latent energy transport reduces the net energy transport to a relatively small value (e.g., Oort 1971; Oort and Peixoto 1983).

To understand the energy transport mechanism, we show in Figs. 2, 3 the vertical profile of $\langle \nabla \cdot (h\mathbf{v}) \rangle$, $\langle (\partial/\partial p)(h\omega) \rangle$, and its constituents. The values in these figures are normalized by c_p, such that the units are in K day^{-1}. A positive value means divergence of heat flux or cooling, while a negative value denotes convergence of heat flux or heating. Within the lower troposphere (below 800 mb), because of the low-level mass convergence of the trade wind, there is a strong horizontal convergence of moist static energy, with a maximum of about −60 K day^{-1}. The dominant contribution comes from sensible heat convergence, although latent energy convergence is also very important. Potential energy convergence is negligible (Fig. 2). The large-scale vertical motion transports the sensible heat and latent energy from the low-level convergence upward to the upper troposphere and converts most latent energy and part of sensible heat into potential energy, accompanied by latent heat release and adiabatic cooling (Fig. 3). This upper-troposphere vertical convergence of sensible heat and potential energy is largely balanced by a strong horizontal divergence (export) of moist static energy out of the WPA, in the form of sensible heat and potential energy (Fig. 2). Since latent energy decreases rapidly with height, horizontal divergence of latent energy decreases significantly in the upper troposphere (e.g., Oort and Peixoto 1983). Considering Table 1 and Figs. 2, 3 together, it is apparent that the net export of moist static energy out of the WPA is a relatively small difference of large horizontal convergence in the lower troposphere and large horizontal divergence in the upper troposphere

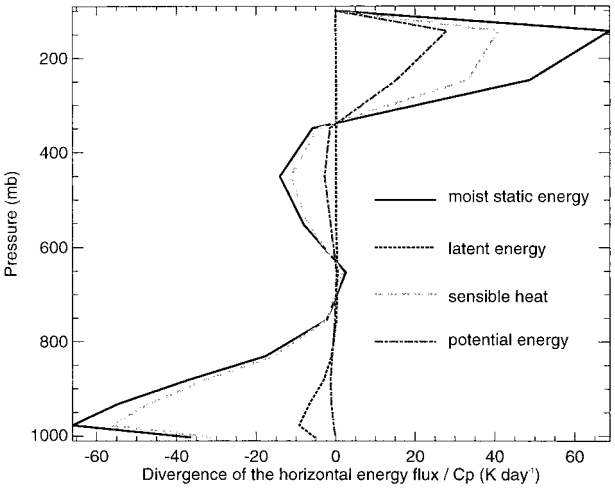

FIG. 2. The 4-month average vertical profile of the monthly mean horizontal divergence of the horizontal large-scale dynamic energy flux in the WPA normalized by c_p.

of moist static energy. The lower troposphere mass horizontal convergence imports both sensible heat and latent energy into the WPA. As the air rises, the horizontally converged moisture condenses, and the associated latent heat release converts latent energy to sensible heat. At the same time, the rising air, which undergoes adiabatic cooling, converts part of its sensible heat to potential energy. When the air reaches the upper troposphere and moves out of the WPA due to mass horizontal divergence, potential energy generated during the ascent as well as the rest of sensible heat is exported. This is consistent with the large-scale heat transport picture suggested by the earlier studies by, for example, Oort (1971) and Oort and Peixoto (1983).

The horizontal and vertical divergence terms shown in Figs. 2 and 3 are combined in Fig. 4 to illustrate the

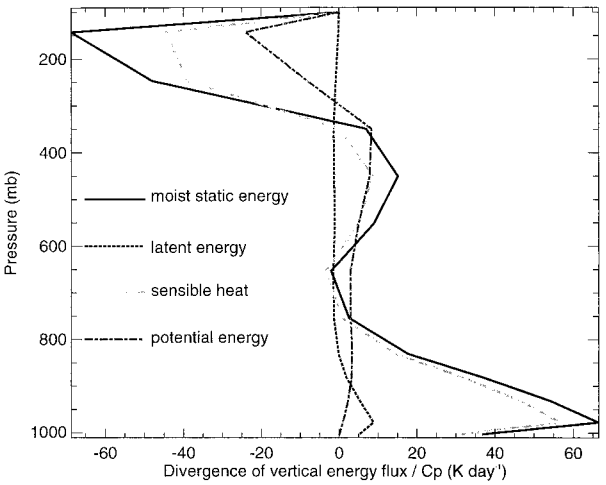

FIG. 3. The 4-month average vertical profile of the monthly mean vertical divergence of the vertical large-scale dynamic energy flux in the WPA normalized by c_p.

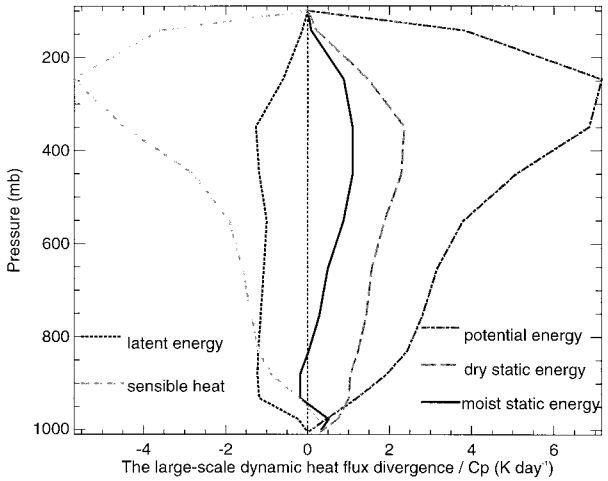

FIG. 4. The 4-month average vertical profile of the monthly mean 3D divergence of the large-scale dynamic heat flux in the WPA normalized by c_p.

net divergence of energy within each atmospheric layer due to the large-scale heat transport. At every level, except the boundary layer, there is a net divergence of moist static energy, resulting in a cooling of the WPA by large-scale motions. The maximum, about 1.2 K day^{-1}, is located in the upper troposphere (200–500 mb). The minimum, about -0.2 K day^{-1}, is located in the boundary layer. When integrated vertically, it represents the net heat transport out of the WPA as given in Table 1. Note that moist static energy is the sum of latent energy, sensible heat, and potential energy and that there is a strong exchange of energy between these three terms and a strong compensation in these three forms of energy transport. This compensation reflects the fact that the latent heat and sensible heat are converted to potential energy in the WP ascending air.

It is of interest to note that the FSU reanalysis suggests that the sensible heat import is greater than the latent energy import (Table 1). This demonstrates that the sensible heat convergence is at least as important as the latent energy convergence in the WP atmospheric heat budget. Our current findings about the sensible heat convergence into the WPA agree very well with those from the earlier studies by Oort (1971), Oort and Peixoto (1983), and Masuda (1988).

b. Heat transport by MMC and TEs

The monthly mean large-scale dynamic heat transport can be partitioned into transport by the MMC and by the TEs:

$$\langle \nabla \cdot \overline{\overline{(h\mathbf{v})}} \rangle = \nabla \cdot \overline{\overline{[\langle h \rangle \langle \mathbf{v} \rangle]}} + \nabla \cdot \overline{\overline{[\langle h^* \mathbf{v}^* \rangle]}}, \quad (13)$$

where $\nabla \cdot \overline{\overline{[\langle h \rangle \langle \mathbf{v} \rangle]}}$ is the monthly mean large-scale dynamic heat transport due to the MMC and $\nabla \cdot \overline{\overline{[\langle h^* \mathbf{v}^* \rangle]}}$ is that due to the TEs. The rhs of Eq. (13) and their contributions from each energetic form are evaluated and summarized in Table 2.

TABLE 2. Contributions to the 4-month average large-scale dynamic energy transport in the WPA from the monthly mean circulation (MMC), and transient eddies (TEs). The unit is W m^{-2}.

	h	Lq	c_pT	ϕ	s
MMC	40	−120	−260	420	160
TEs	20	20	0	0	0

The major part of the large-scale heat transport out of the WPA is accomplished by the MMC, that is, the large-scale overturning associated with the divergent wind component in the Hadley circulation and Walker circulation. The MMC exports about 40 W m^{-2} energy, that is, about 70% of the total heat export, whereas the TEs export about 20 W m^{-2} energy, about 30% of the total energy transport, out of the WPA. The lower branch of the MMC imports both latent energy (about -120 W m^{-2}) and sensible heat (about -260 W m^{-2}) into the WPA, while the upper branch of the MMC exports potential energy (about 420 W m^{-2}) out of the WPA. The TEs mainly transport the latent energy out of the WPA, which is opposite to the MMC latent energy transport (e.g., Masuda 1988). The TEs transport of sensible heat and potential energy is almost zero (e.g., Riehl and Malkus 1958). Overall, the role of the TEs in the large-scale dynamic heat transport is small but still important in the WPA. These results agree very well with the conclusions from earlier studies by, for example, Oort (1971), Oort and Peixoto (1983), Masuda (1988), Trenberth and Solomon (1994) for the Tropics.

c. Spatial variations

Figures 5a–e show the horizontal distribution of the large-scale transport of moist static energy, dry static energy, latent energy, sensible heat, and potential energy. As anticipated from Figs. 2, 3, and 4, in most regions of the WP, there is a net divergence of moist static energy, dry static energy and potential energy, and a net convergence of latent energy and sensible heat. The maximum is approximately located between 5°N and 5°S, where the highest SST is found. In the northern part of the WP, that is, between 5° and 10°N, where there is a strong SST gradient and relatively cold SST (below 301.5 K), there is a divergence of latent energy plus sensible heat and a convergence of potential energy. The spatial pattern of dry static energy transport is supported by Lin and Johnson (1996), who showed that there is a precipitation maximum near (160°E, 5°S), (170°E, 5°N), and 5°N west of 160°E during the TOGA COARE intensive observing period (IOP). Our study shows that there are strong spatial variations in the large-scale heat transport in the WP during TOGA COARE and CEPEX. This is consistent with Lin and Johnson (1996), Godfrey et al. (1998), Curry et al. (1999), Chou et al. (2000), and Johnson and Ciesielski (2000), who

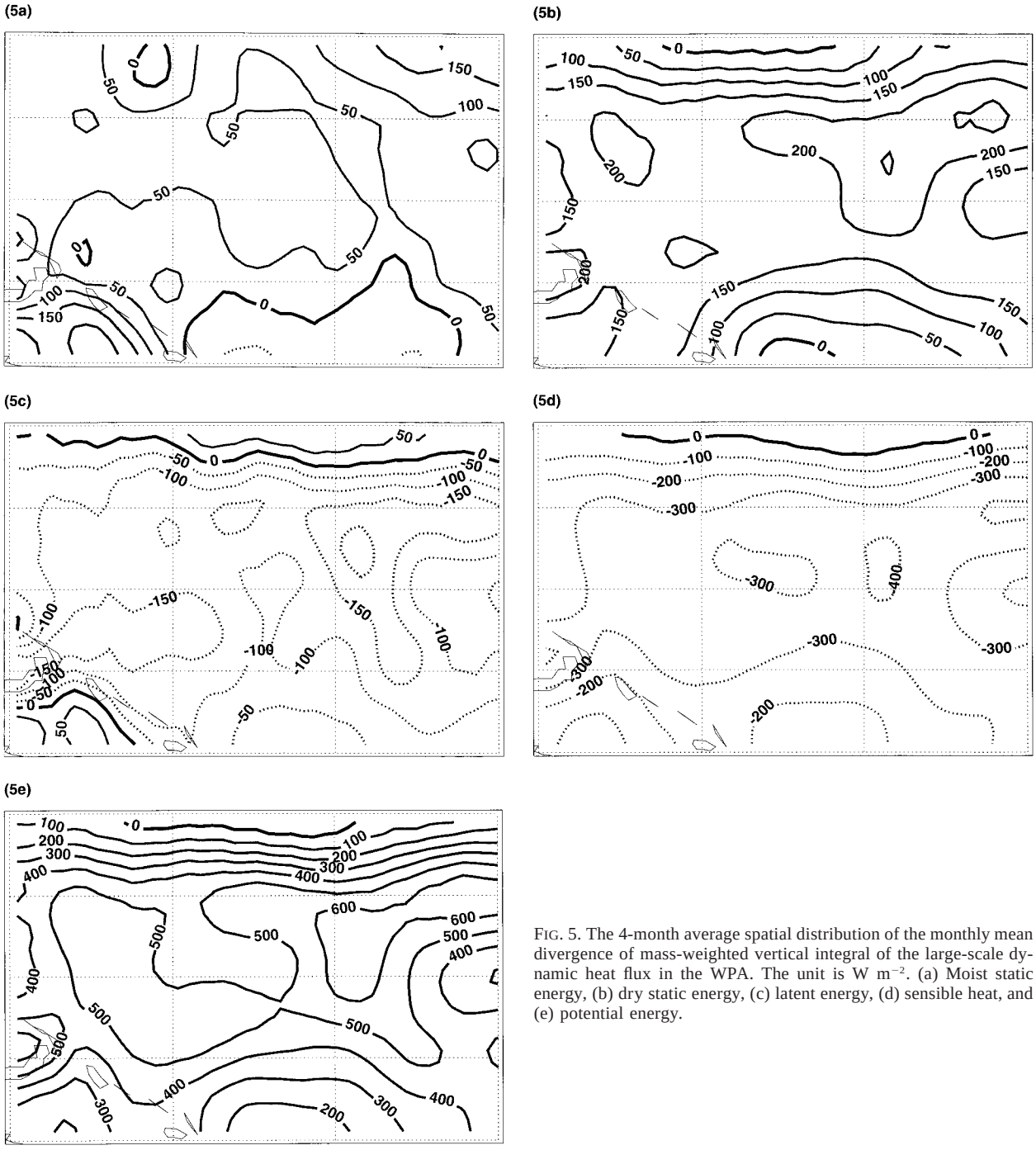

FIG. 5. The 4-month average spatial distribution of the monthly mean divergence of mass-weighted vertical integral of the large-scale dynamic heat flux in the WPA. The unit is W m^{-2}. (a) Moist static energy, (b) dry static energy, (c) latent energy, (d) sensible heat, and (e) potential energy.

also show that there are strong spatial variations in SST, deep convection, cloud, latent heat release, and the surface heat fluxes.

As seen in the total heat budget equations (4) and (9), the atmospheric moist static energy export is balanced by the mass-weighted vertical integral of the apparent total heat source in the atmosphere, in other words, the surface turbulent heat flux and the net radiative flux into the atmosphere. As will be seen later in section 5, the clear sky radiation has a strong cooling effect in the WPA. The moist static energy transport by the large-scale circulation in the WPA is entirely from the direct convective heating $\overline{\langle Q_C \rangle}$ and the indirect convective heating. Because of both the direct and indirect convective heating, there is a radiative-convective disequilibrium, that is, the convective heating exceeds the radiative cooling, which provides a net apparent total heat source for the WPA. Induced by the apparent total heat

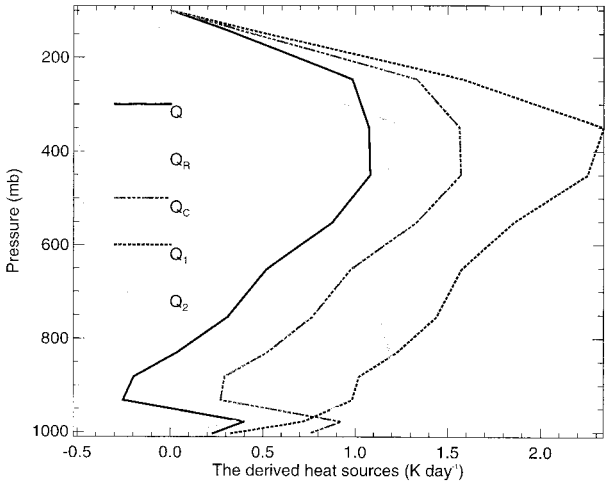

FIG. 6. The 4-month average vertical profile of the monthly mean apparent total heat source Q, apparent heat source Q_1, apparent moisture sink Q_2, radiative heating Q_R, and convective heating Q_C in the WPA normalized by c_p.

source, the air ascends nonmoist adiabatically and exports the heat out of the WPA. Therefore to understand the large-scale dynamic heat transport, the detailed analysis of both the direct and the indirect convective heating is required.

5. Derived heat sources

As discussed in section 4, the large-scale circulation cools the WPA. There must exist an energy source for the WPA to maintain its equilibrium because the heat storage is negligible in the period of this study [Eqs. (4) and (5)]. The apparent total heat source Q inferred from the large-scale dynamic heat transport and its contributions from radiation and convection are examined in this section.

a. Apparent total heat source

Figure 6 recasts the results in Fig. 4 in terms of the apparent total heat source. The strong dynamic cooling indicates that there is a strong, positive apparent total heat source at all levels except the boundary layer (Fig. 6). Since the area and the period of the present study largely coincides with those of TOGA COARE, the apparent heat source Q_1 and the apparent moisture sink Q_2 are also calculated using Eqs. (1) and (3) from the FSU reanalysis and can be compared with those from TOGA COARE by Lin and Johnson (1996), Frank et al. (1996), and Johnson and Ciesielski (2000). We note that there are some qualitative similarities in both Q_1 and Q_2 profiles. Here Q_1 is positive throughout the troposphere with a maximum of about 2.3 K day^{-1} near the 400-mb level (Fig. 6), and Q_2 has two weak peaks below 900 mb and above 400 mb, and a single minimum about 1 K day^{-1} near 600 mb (Fig. 6). The maximum magnitudes of Q_1 and Q_2 are also very similar to the LSA values from Frank et al. (1996), but are smaller than the outer sounding array (OSA) and the intensive flux array (IFA) values from the COARE studies. This is consistent with the strong spatial variations of the energy transport as we show in section 4c.

b. Radiative heating

During the TOGA COARE and CEPEX period, the average ERBE WFOV WPA TOA net downward radiative flux is about 110 W m^{-2}. The uncertainties are about 10 W m^{-2} (Rieland and Raschke 1991, see discussion in Trenberth and Solomon 1994). During IOP, the 4-month average WP surface net downward radiative flux is about 145 W m^{-2} with uncertainties of about 30 W m^{-2} according to the TOGA COARE observations (Chou et al. 1998). The WP surface net downward radiative flux on March 1993 is about 180 W m^{-2} with uncertainties of about 30 W m^{-2} from the CEPEX observations (Collins et al. 1996). The approximate average of COARE and CEPEX value, which is about 150 W m^{-2} with uncertainties of about 30 W m^{-2}, is used as our estimate of the 4-month average WP surface net downward radiative flux. Since the available observational radiation data do not give the radiative heating profile, Dopplick's (1979) tropical (10°N–10°S) radiative heating profile is adopted and normalized by the WPA radiation fluxes from ERBE, COARE, and CEPEX, as our final estimate. It should be noted that we only use Dopplick's (1979) vertical profile, but not his absolute value.

The radiative heating rate in the WPA is only about -0.4 K day^{-1}, which is equivalent to a radiation flux convergence of -40 W m^{-2} with uncertainties of about 30 W m^{-2}. This number agrees very well with the radiative heating rate in IFA or outer sounding array during IOP by the independent studies of T. Ackerman (cited in Frank et al. 1996) and Johnson and Ciesielski (2000) from the atmospheric budget (their Table 5). When compared with the other previous radiation flux convergence estimates in the Tropics, for example, -110 W m^{-2} by Dopplick (1979), -110 W m^{-2} by Cox and Griffith (1979), and -90 W m^{-2} by Thompson et al. (1979), the radiative cooling in the WPA is dramatically smaller. This difference is largely due to the CRF associated with the deep convective cirrus clouds in the WPA (e.g., Stephens et al. 1994; Collins et al. 1996; Bergman and Hendon 1998; Chou et al. 1998; Sohn 1999). The deep convective clouds compensate the larger clear sky radiative cooling and warm the atmosphere mainly through the longwave cloud forcing and partly due to the cloud solar absorption. If we adopt the whole tropical clear sky radiative flux convergence of about -110 W m^{-2} by Dopplick (1979) (see Johnson and Ciesielski 2000) for the WPA, then the WPA CRF is about 70 W m^{-2}.

In addition to warming the atmosphere through the

longwave cloud forcing, the CRF of the deep convective clouds also cools the surface through the shortwave cloud forcing (e.g., Ramanathan and Collins 1991; Collins et al. 1996; Waliser et al. 1996; Chou et al. 1998). TOGA COARE and CEPEX observations show that the CRF at the surface is about 80–100 W m^{-2} in the WP (Collins et al. 1996; Waliser et al. 1996; Chou et al. 1998). So, although the deep convective clouds have nearly zero effect on the WP atmosphere–ocean column heat budget at the TOA (e.g., Ramanathan et al. 1989; Ramanathan and Collins 1991; Collins et al. 1996), they have a strong warming effect in the atmosphere and a strong cooling effect at the surface. This dipole structure is quite similar to the profile of the convective heating Q_C, as we will discuss in section 5c. It is appropriate then to refer to the CRF of the deep convective clouds as the ''indirect convective heating,'' and Q_C as the direct convective heating. Like the direct convective heating, the CRF of the deep convective clouds enhances the required atmospheric heat transport and reduces the required oceanic heat transport significantly in the WP. This finding agrees very well with the earlier study by Zhang and Rossow (1997).

c. Convective heating

Although the CRF of the deep convective clouds provides a strong heat source for the WPA, the net radiation is still a heat sink. This radiative cooling in addition to the dynamic cooling inferred from section 4 must be balanced by the convective heating [Eq. (5), Riehl and Malkus 1958]. The moist convection, in the form of undiluted hot towers, transports moist static energy from the ocean surface to the atmosphere through direct convective heating, that is, the vertical eddy sensible heat and latent energy transport. Figure 6 shows that the inferred convective heating is around 1 K day^{-1}. The maximum is about 1.6 K day^{-1} and located in the upper troposphere between 300 and 600 mb. The minimum is about the 0.3 K day^{-1} and located at 950 mb, corresponding to the lower peak of Q_2. The mass-weighted vertical integral of the convective heating is equal the surface turbulent heat fluxes, which are about 100 W m^{-2}.

The vertical distribution shows that the moist convection provides a net source of moist static energy throughout the troposphere. This vertical structure is consistent with Johnson and Ciesielski (2000), in which Q_C is expected to be positive throughout the troposphere. On the other hand, an earlier study by Emanuel (1994), which estimated Q_C from the GARP Atlantic Tropical Experiment data, shows that convection provides a net sink of moist static energy in the lower troposphere. Several causes may be contributed to this difference. First, different Q_R data and profile are used in these two studies (Cox and Griffith 1979). Second, maybe more importantly, the discrepancy may be due to the different location, horizontal scale, and season considered in these two studies.

d. Overall energy cycle

After analyzing the heat sources and sinks in the WPA, we summarize the overall WP atmospheric energy cycle below. The net input solar radiation from the TOA is largely absorbed by the ocean surface and subsequently transferred to the atmosphere by thermal radiation. Through the complex process of the clear sky absorber gases and radiation interaction, there is a net radiative heating at the ocean surface and a net radiative cooling in the atmosphere (e.g., Kiehl and Trenberth 1997). This is inductive to moist convection. Then the atmosphere is heated indirectly by both the direct convective heating and the indirect convective heating. Globally, the atmosphere is in radiative-convective equilibrium (Kiehl and Trenberth 1997), but locally, for example, in the WPA, there is a radiative-convective disequilibrium, that is, the convective heating exceeds the radiative cooling, which provides a net apparent total heat source for the WPA. We should point out here that radiative-convective disequilibrium is due to both the direct and indirect convective heating.

The apparent total heat source induces the moist thermodynamically direct large-scale circulation, which imports sensible heat and latent energy into the WPA through the low-level mass convergence. This imported energy together with the energy from the apparent total heat source is then transported upward to the upper troposphere. During the upward transport most latent energy is converted into sensible heat through the latent heat release and some sensible heat is converted into potential energy through the large-scale adiabatic cooling. In the upper-outflow branch of the Hadley and Walker circulation, the potential energy and sensible heat are exported out of the WPA to the subtropics or cold tongue through the large-scale mass divergence. Obviously the WP air undergoes the nonmoist adiabatic process, which makes the heat transport possible. Finally, the total atmospheric heat transport by the large-scale circulation equals to the apparent total heat source, and the WPA reaches a state of radiative-convective-dynamic equilibrium.

The sources and sinks for each energy form in the WPA are summarized below. The sources for latent energy are the surface latent heat flux and the net large-scale convergence. The sink is the latent heat release, which converts latent energy to sensible heat. The latent heat release dominates the latent energy budget [Eqs. (3) and (8)]. There are three sources for sensible heat: the net large-scale convergence, the surface sensible heat flux, and the latent heat release. The sinks for sensible heat are the radiative cooling and adiabatic cooling associated with the large-scale vertical motion, which converts sensible heat to potential energy. The adiabatic cooling dominates the sensible heat budget [Eqs. (1)

TABLE 3. The 4-month average observed precipitation (LP), latent heat flux (LE), sensible heat flux (SH), radiative heat flux at TOA (R_T), and surface (R_S) and their uncertainties in the WPA from ERBE, TOGA COARE, TOGA TAO, and CEPEX. The unit is W m^{-2}.

Fields	Observed value	Uncertainties	Observational source
LP	250	60	GPCP
LE	110	30	TAO
SH	10	5	TAO
R_T	110	10	ERBE
R_S	150	30	COARE, CEPEX

TABLE 4. The 4-month average mass-weighted vertical integral of the apparent heat source $\overline{\overline{Q_1}}$, the apparent moisture sink $\overline{\overline{Q_2}}$, and the apparent total heat source $\overline{\overline{Q}}$ in the WPA from the FSU reanalysis and observations. The unit is W m^{-2}.

Fields	FSU reanalysis	Observations and uncertainties	Observational sources
$\overline{\overline{Q_1}}$	160	220 (60)	ERBE, COARE, CEPEX, GPCP, TAO
$\overline{\overline{Q_2}}$	100	140 (60)	GPCP, TAO
$\overline{\overline{Q}}$	60	80 (30)	ERBE, COARE, CEPEX, TAO

and (6)]. The source for potential energy is the conversion from sensible heat due to the adiabatic cooling associated with the large-scale vertical motion and the sink is the large-scale export in the upper-outflow branch of the Hadley and Walker circulation [Eqs. (2) and (7)].

6. Uncertainties in the data and analyses

To evaluate the quality of our budget calculation, we utilize the observations from the surface and satellite. For the convenience of discussion, we will rewrite Eqs. (6), (8), (9) here:

$$\overline{\overline{Q_1}} = R_T - R_S + \mathrm{LP} + \mathrm{SH}, \tag{6a}$$

$$\overline{\overline{Q_2}} = \mathrm{LP} - \mathrm{LE}, \tag{8a}$$

$$\overline{\overline{Q}} = R_T - R_S + \mathrm{LE} + \mathrm{SH}. \tag{9a}$$

The rhs terms are observable quantities and the lhs terms are the apparent heat source, apparent moisture sink, and the apparent total heat source calculated from the reanalysis data. To the extent that the observed fields are accurate, the difference between the lhs and rhs would provide an overall check on the quality of the reanalysis data and the uncertainties of the budget calculation. In light of this approach, Table 4 shows the lhs and rhs terms of Eqs. (6a), (8a), and (9a), respectively. The observed values of the individual term on rhs are given in Table 3. The radiation fluxes are estimated from the ERBE TOA, TOGA COARE, and CEPEX surface radiation data. The precipitation is evaluated from the GPCP version 1a combined precipitation (Huffman et al. 1997). The surface latent and sensible heat fluxes are calculated based on the TOGA TAO moored buoys data (Zhang and McPhaden 1995).

First we discuss the uncertainties in our ''observational'' estimates of $\overline{\overline{Q_1}}$, $\overline{\overline{Q_2}}$, and $\overline{\overline{Q}}$. As discussed in section 5b, the uncertainties in the radiative flux into the WPA from ERBE, COARE, and CEPEX are about 30 W m^{-2}. Gleckler and Weare (1997) have demonstrated that the uncertainties in Oberhuber's (1988) surface turbulent heat flux are about 30 W m^{-2} in the tropical Pacific mainly due to the systematic errors in bulk formulas. Since we have used the more accurate TOGA TAO moored buoy data, 30 W m^{-2} uncertainty is an upper limit for the present estimates. As a result, the uncertainties in our observational estimates of $\overline{\overline{Q}}$, and accordingly the atmospheric and oceanic energy transport, are about 30 W m^{-2}. Although various approaches have been attempted to estimate the precipitation in the WP during TOGA COARE, the estimated precipitation can still vary from 150 to 300 W m^{-2} (e.g., Frank et al. 1996; Lin and Johnson 1996; Johnson and Ciesielski 2000). This indicates the high variability of rainfall in the WP and the difficulties of obtaining an accurate estimate. The GPCP employs four methods to estimate the rainfall, but 60 W m^{-2} uncertainties are expected in the WP. Thus, the uncertainties in our ''observational'' estimate of $\overline{\overline{Q_1}}$ and $\overline{\overline{Q_2}}$ are about 60 W m^{-2} because of the large uncertainties in the GPCP precipitation. Although large uncertainties exist in the observational estimates of $\overline{\overline{Q_1}}$, $\overline{\overline{Q_2}}$, and $\overline{\overline{Q}}$, they are still useful as a benchmark for our energy budget calculation from the FSU reanalysis.

The observed $\overline{\overline{Q}}$ (through the radiative fluxes at the TOA and the surface, and the latent and sensible heat fluxes at the surface) is about 80 W m^{-2}, while our budget estimated $\overline{\overline{Q}}$, which is moist static energy transport in the WPA, is about 60 W m^{-2}. The difference is within the uncertainties of the observed $\overline{\overline{Q}}$, which suggests that $\overline{\overline{Q}}$ and moist static energy transport is quite accurate in our budget calculation. But we find that large differences exist between the observed and our budget estimated $\overline{\overline{Q_1}}$ and $\overline{\overline{Q_2}}$. It may be that both $\overline{\overline{Q_1}}$ and $\overline{\overline{Q_2}}$ are underestimated in our budget calculation such that their difference (i.e., $\overline{\overline{Q}}$) is comparable to the observations. Or the GPCP precipitation is overestimated because of difficulties in ''measuring'' the WP rainfall (Johnson and Ciesielski 2000). Since our budget estimated $\overline{\overline{Q_1}}$ and $\overline{\overline{Q_2}}$ are very close to those by Trenberth and Solomon (1994), we believe that it is more likely the large errors in the GPCP precipitation are responsible for these large differences between the observed and our budget estimated $\overline{\overline{Q_1}}$ and $\overline{\overline{Q_2}}$.

7. Summary

The principal results of this study and the overall heat budget in the WPA during the TOGA COARE and CE-

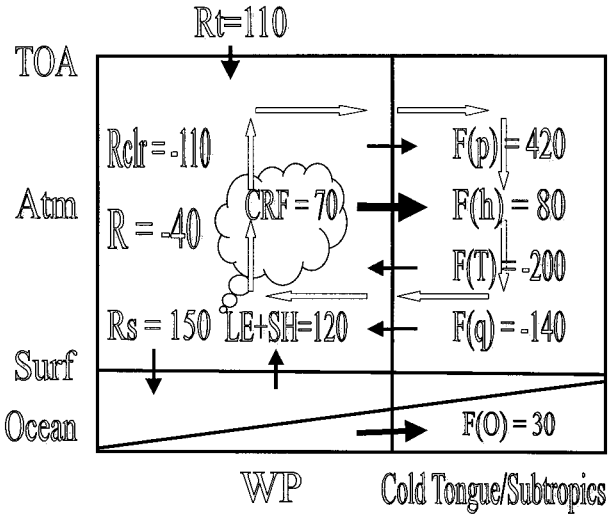

FIG. 7. The 4-month average overall heat budget in the WPA during the TOGA COARE and CEPEX period from Dec 1992 to Mar 1993. Here $F(h)$ is the atmospheric heat transport; $F(p)$, $F(T)$, and $F(q)$ are its contribution from potential energy, sensible heat, and latent energy, respectively; $F(O)$ is the oceanic heat transport; and R and R_{clr} are the cloudy sky and clear sky radiative flux convergence separately. CRF is the cloud radiative forcing (CRF). The data sources are as follows: ERBE for R_T; TOGA COARE and CEPEX for R_S; $R = R_T - R_S$; R_{clr}, see text; CRF $= R - R_{\text{clr}}$; TOGA TAO for LE + SH; $\overline{F(h)}$ from Table 4; $\overline{F(p)}$ from Table 1; $\overline{F(q)}$ from Table 4; $\overline{F(T)} = \overline{Q_1} - \overline{F(p)}$, while $\overline{Q_1}$ from Table 4.

PEX period from December 1992 to March 1993 are summarized schematically in Fig. 7.

The net downward radiative flux at the TOA is about 110 W m^{-2} with uncertainties of about 10 W m^{-2}. The net downward heat flux at the ocean surface, in other words, the required oceanic heat transport if heat storage is neglected, is about 30 W m^{-2} with uncertainties of the same magnitude. The net heat flux at the surface is higher than the in situ buoy and ship measurement from Weller and Anderson (1996), the satellite-derived value from Chou et al. (2000), and smaller than the satellite-derived value from Curry et al. (1999). But it agrees very well with recent blended estimation from Zhang et al. (2000). Accordingly the required atmospheric heat transport is about 80 W m^{-2} with uncertainties of about 30 W m^{-2}. The uncertainties in the air–sea heat fluxes and the atmospheric and oceanic heat transport are still large and more work is needed (see more discussion in Godfrey et al. 1998).

The large-scale circulation imports about 140 W m^{-2} latent energy and about 200 W m^{-2} sensible heat with uncertainties of about 60 W m^{-2} into the WPA, mainly through the low-level mass convergence. The large-scale circulation exports about 420 W m^{-2} potential energy with uncertainties of about 60 W m^{-2} out of the WPA, mainly by the upper-level mass divergence. The individual energy transport is large, however the strong compensation between potential energy transport and sensible heat plus latent energy transport reduces the net energy transport to a relatively small value (e.g., Oort 1971; Oort and Peixoto 1983). The net effect of the large-scale circulation is to export about 80 W m^{-2} moist static energy with uncertainties of about 30 W m^{-2} out of the WPA, which corresponds to an average cooling rate of about 0.8 K day^{-1} in the whole troposphere. About 70% of the large-scale dynamic heat transport in the WPA is done by the MMC, that is, the large-scale overturning associated with the divergent wind component as manifest in the Hadley and Walker circulation. The TEs play a small role in the WPA large-scale dynamic heat transport. When compared to the radiative cooling rate in the WPA, the large-scale circulation is very efficient in exporting heat and plays a vital role in the WP atmospheric heat balance. So our current findings confirm the assumption of efficient atmospheric heat transport that was used by several earlier studies concerning the regulation of SST in the WP, for example, Ramanathan and Collins (1991), Fu et al. (1992), Wallace (1992), Hartmann and Michelsen (1993), Lau et al. (1994), and Pierrehumbert (1995).

As pointed out by Riehl and Malkus (1958), the heat source for the WPA is the moist convection, which transports moist static energy from the ocean surface to the atmosphere through the direct convective heating, that is, the vertical eddy sensible heat and latent energy transport. So the direct convective heating has a dipole structure, in other words, strong heating of the atmosphere and strong cooling of the surface. As a result, the moist convection enhances the atmospheric heat transport and reduces the oceanic heat transport in the WP. The moist convection heats the atmosphere at a rate of about 1.2 K day^{-1}, including both the upper and the lower troposphere. The vertical integral of the direct convective heating is equal to the surface turbulent heat flux. The value is about 120 W m^{-2} with uncertainties of about 30 W m^{-2}, which agrees very well with the in situ buoy and ship measurement from Weller and Anderson (1996).

The radiative heating rate in the WPA is only about -0.4 K day^{-1}, which is equivalent to a radiation convergence of about -40 W m^{-2} with uncertainties of about 30 W m^{-2}. When compared with the other previously cited radiation flux convergence in the Tropics, the radiative cooling in the WPA is dramatically smaller. This difference is largely due to the CRF, about 70 W m^{-2}, associated with the deep convective cirrus clouds in the WPA, which compensates the larger clear sky radiative cooling, about -110 W m^{-2}. Thus moist convection heats the WPA, not only through the direct convective heating, but also through the indirect convective heating, that is, the CRF of the deep convective clouds. The CRF of the deep convective clouds has the same dipole structure as the direct convective heating. As a result, CRF of the deep convective clouds enhance the atmospheric heat transport and reduce the oceanic heat transport significantly in the WP.

Overall as expected, the WPA is in a state of radiative-

convective-dynamic equilibrium, that is, the convective heating balances the radiative cooling and the dynamic cooling [Eq. (5)]. A more detailed understanding of both convection and radiation, especially the direct and indirect convective heating, is required to deeply understand the large-scale atmospheric heat transport and atmospheric general circulation in the Tropics.

Acknowledgments. We thank Dr. P. J. Rasch, Dr. W. D. Collins, Mr. B. Eaton at the National Center for Atmospheric Research (NCAR), Dr. T. N. Krishnamurti at Florida State University, and Dr. G. J. Huffman at Goddard Space Flight Center for their assistance on the needed data. We sincerely thank two anonymous reviewers for their thorough reviews and helpful comments. We also want to express our deep gratitude to Dr. K. E. Trenberth for taking time to read the manuscript and pointing out a major inconsistency in an earlier version of this paper. Incorporation of his suggested correction to our analysis significantly improved the accuracy of our estimate. This research was supported by the Environmental Science Division of U.S. Department of Energy under Grant DEFG 0391 ER 61198 as part of the Atmospheric Radiation Measurement Program and by the National Science Foundation under Grants ATM9405024 and ATM9525800. This paper is Report 218 of the Center for Clouds, Chemistry and Climate (C4).

REFERENCES

Arkin, P. A., and P. Xie, 1994: The Global Precipitation Climatology Project: First Algorithm Intercomparison Project. *Bull. Amer. Meteor. Soc.,* **75,** 401–419.

Barkstrom, B. R., 1984: The Earth Radiation Budget Experiment (ERBE). *Bull. Amer. Meteor. Soc.,* **65,** 1170–1185.

Bergman, J. W., and H. H. Hendon, 1998: Calculating monthly radiative fluxes and heating rates from monthly cloud observations. *J. Atmos. Sci.,* **55,** 3471–3491.

Chou, M.-D., W. Zhao, and S. H. Chou, 1998: Radiation budgets and cloud radiative forcing in the Pacific warm pool during TOGA COARE. *J. Geophys. Res.,* **103,** 16 967–16 977.

Chou, S. H., W. Zhao, and M.-D. Chou, 2000: Surface heat budgets and sea surface temperature in the Pacific warm pool during TOGA COARE. *J. Climate,* **13,** 634–649.

Collins, W. D., F. P. J. Valero, P. J. Flatau, D. Lubin, H. Grassl, and P. Pilewskie, 1996: Radiative effects of convection in the tropical Pacific. *J. Geophys. Res.,* **101,** 14 999–15 012.

Cox, S. K., and K. T. Griffith, 1979: Estimates of radiative divergence during Phase III of the GARP Atlantic Tropical Experiment: Part II. Analysis of Phase III results. *J. Atmos. Sci.,* **36,** 586–601.

Curry, J. A., C. A. Clayson, W. B. Rossow, R. Reeder, Y.-C. Zhang, P. J. Webster, G. Liu, and R.-S. Sheu, 1999: High-resolution satellite-derived dataset of the surface fluxes of heat, freshwater, and momentum for the TOGA COARE IOP. *Bull. Amer. Meteor. Soc.,* **80,** 2059–2080.

Dopplick, T. G., 1979: Radiative heating of the global atmosphere: Corrigendum. *J. Atmos. Sci.,* **36,** 1812–1817.

Emanuel, K. A., 1994: *Atmospheric Convection.* Oxford University Press, 580 pp.

Frank, W. M., H. Wang, and J. L. McBride, 1996: Rawinsonde budget analyses during the TOGA COARE IOP. *J. Atmos. Sci.,* **53,** 1761–1780.

Fu, R., A. D. Del Genio, W. B. Rossow, and W. T. Liu, 1992: Cirrus-cloud thermostat for tropical sea surface temperature tested using satellite data. *Nature,* **358,** 394–397.

Gairola, R. K, and T. N. Krishnamurti, 1992: Rain rates based on SSM/I, OLR and rain gauge data sets. *Meteor. Atmos. Phys.,* **50,** 165–174.

Gleckler, P. J., and B. C. Weare, 1997: Uncertainties in global ocean surface heat flux climatologies derived from ship observations. *J. Climate,* **10,** 2764–2781.

Godfrey, J. S., R. A. Houze Jr., R. H. Johnson, R. Lukas, J.-L. Redelsperger, A. Sumi, and R. Weller, 1998: Coupled Ocean Atmosphere Response Experiment (COARE): An interim report. *J. Geophys. Res.,* **103,** 14 395–14 450.

Hartmann, D. L., and M. L. Michelsen, 1993: Large-scale effects on the regulation of tropical sea surface temperature. *J. Climate,* **6,** 2049–2062.

Hayes, S. P., L. J. Mangum, J. Picaut, A. Sumi, and K. Takeuchi, 1991: TOGA–TAO: A moored array for real-time measurements in the tropical Pacific Ocean. *Bull. Amer. Meteor. Soc.,* **72,** 339–347.

Huffman, G. J., and Coauthors, 1997: The Global Precipitation Climatology Project (GPCP) combined precipitation data set. *Bull. Amer. Meteor. Soc.,* **78,** 5–20.

Johnson, R. H., and P. E. Ciesielski, 2000: Rainfall and radiative heating rates from TOGA COARE atmospheric budgets. *J. Atmos: Sci.,* **57,** 1497–1514.

Kiehl, J. T., and K. E. Trenberth, 1997: Earth's annual global mean energy budget. *Bull. Amer. Meteor. Soc.,* **78,** 197–208.

Krishnamurti, T. N., J. Xue, H. S. Bedi, K. Ingles, and D. Oosterhof, 1991: Physical initialization for numerical weather prediction over the Tropics. *Tellus,* **43AB,** 53–81.

——, B. Jha, P. J. Rasch, and V. Ramanathan, 1997: A high-resolution global reanalysis highlighting the winter monsoon. Part I: Reanalysis fields. *Meteor. Atmos. Phys.,* **64,** 123–150.

Lau, K.-M., C.-H. Sui, M.-D. Chou, and W.-K. Tao, 1994: An inquiry into the cirrus-cloud thermostat effect for tropical sea surface temperature. *Geophys. Res. Lett.,* **21,** 1157–1160.

Lin, X., and R. H. Johnson, 1996: Heating, moistening, and rainfall over the western Pacific warm pool during TOGA COARE. *J. Atmos. Sci.,* **53,** 3367–3383.

Masuda, K., 1988: Meridional heat transport by the atmosphere and the ocean: Analysis of FGGE data. *Tellus,* **40A,** 285–302.

Oberhuber, J. M., 1988: An atlas based on ''COADS'' dataset: The budgets of heat, buoyancy and turbulent kinetic energy at the surface of the global ocean. Max-Planck-Institute for Meteorology Rep. 15, 199 pp.

Oort, A. H., 1971: The observed annual cycle in the meridional transport of atmospheric energy. *J. Atmos. Sci.,* **28,** 325–339.

——, and J. P. Peixoto, 1983: Global angular momentum and energy balance requirements from observations. *Advances in Geophysics,* Vol. 25, Academic Press, 355–490.

Peixoto, J. P., and A. H. Oort, 1992: *Physics of Climate.* American Institute of Physics, 520 pp.

Pierrehumbert, R. T., 1995: Thermostats, radiator fins and local runaway greenhouse. *J. Atmos. Sci.,* **52,** 1784–1806.

Ramanathan, V., and W. Collins, 1991: Thermodynamic regulation of the ocean warming by the cirrus clouds deduced from observations of the 1987 El Niño. *Nature,* **351,** 27–32.

——, R. D. Cess, E. F. Harrison, P. Minnis, B. R. Barkstrom, E. Ahmad, and D. Hartmann, 1989: Cloud-radiative forcing and climate: Results from the Earth Radiation Budget Experiment. *Science,* **243,** 57–63.

——, R. Dirks, R. Grossman, A. Heymsfield, J. Kuttner, and F. P. J. Valero, 1993: *Central Equatorial Pacific Experiment Design.*

Center for Cloud, Chemistry and Climate, University of California, San Diego.

Riehl, H., and J. S. Malkus, 1958: On the heat balance in the equatorial trough zone. *Geophysica,* 503–537.

——, and J. (Malkus) Simpson, 1979: The heat balance in the equatorial trough zone, revisited. *Contrib. Atmos. Phys.,* **52,** 287–305.

Rieland, M., and E. Raschke, 1991: Diurnal variability of the earth radiation budget: Sampling requirements, time integration aspects and error estimates for the Earth Radiation Budget Experiment. *Theor. Appl. Climatol.,* **44,** 9–24.

Sohn, B.-J., 1999: Cloud-induced infrared radiative heating and its implications for the large-scale tropical circulation. *J. Atmos. Sci.,* **56,** 2657–2672.

Stephens, G. L., A. Slingo, M. J. Webb, P. J. Minnett, P. H. Daum, L. Kleinman, I. Wittmeyer, and D. A. Randall, 1994: Observations of the earth's radiation budget in relation to atmospheric hydrology. 4: Atmospheric column radiative cooling over the world's ocean. *J. Geophys. Res.,* **99,** 18 585–18 604.

Thompson, R. M., S. W. Payne, E. E. Recker, and R. J. Reed, 1979: Structure and properties of synoptic-scale wave disturbances in the intertropical convergence zone of the eastern Atlantic. *J. Amos. Sci.,* **36,** 53–72.

Trenberth, K. E., 1997: Using atmospheric budgets as a constraint on surface fluxes. *J. Climate,* **10,** 2796–2809.

——, and A. Solomon, 1994: The global heat balance: Heat transports in the atmosphere and ocean. *Climate Dyn.,* **10,** 107–134.

Waliser, D. E., W. D. Collins, and S. P. Anderson, 1996: An estimate of the surface shortwave cloud forcing over the western Pacific during TOGA COARE. *Geophys. Res. Lett.,* **23,** 519–522.

Wallace, J. M., 1992: Effect of deep convection on the regulation of tropical sea surface temperature. *Nature,* **357,** 230–231.

Webster, P. J., and R. Lukas, 1992: TOGA COARE: The Coupled Ocean Atmosphere Response Experiment. *Bull. Amer. Meteor. Soc.,* **73,** 1377–1416.

Weller, R. A., and S. P. Anderson, 1996: Surface meteorology and air–sea fluxes in the western equatorial Pacific warm pool during the TOGA Coupled Ocean–Atmosphere Response Experiment. *J. Climate,* **9,** 1959–1992.

Yanai, M., and T. Tomita, 1998: Seasonal and interannual variability of atmospheric heat sources and moisture sink as determined from NCEP–NCAR reanalysis. *J. Climate,* **11,** 463–482.

——, S. Esbensen, and J. Chu, 1973: Determination of bulk properties of tropical cloud clusters from large-scale heat and moisture budget. *J. Atmos. Sci.,* **30,** 611–627.

Zhang, G., and M. J. McPhaden, 1995: The relationship between sea surface temperature and latent heat flux in the equatorial Pacific. *J. Climate,* **8,** 589–605.

Zhang, S., A. J. Plueddemann, S. P. Anderson, and R. A. Weller, 2000: Surface fluxes and their influence on sea surface temperature in the western equatorial Pacific during COARE. *J. Geophys. Res.,* **105,** 6341–6358.

Zhang, Y.-C., and W. B. Rossow, 1997: Estimating meridional energy transports by the atmospheric and oceanic general circulations using boundary fluxes. *J. Climate,* **10,** 2358–2373.